PARTICLE PRODUCTION IN SOFT HADRON-HADRON, HADRON-NUCLEUS AND NUCLEUS-NUCLEUS COLLISIONS IN A DUAL MONTE-CARLO MULTI-CHAIN FRAGMENTATION MODEL*

BY S. RITTER

Sektion Physik, Karl-Marx-Universität Leipzig, DDR

(Received September 21, 1984)

A dual Monte-Carlo two-chain fragmentation model for hadron-hadron collisions as well as its extension to a multi-chain fragmentation model for hadron-nucleus and nucleus--nucleus collisions is presented. Using a Monte-Carlo method allows the study of inclusive and exclusive quantities. Energy momentum and all additive quantum numbers are conserved exactly in the model. Satisfactory agreement with recent data is obtained.

PACS numbers: 12.40.-y, 13.85.-t

1. Introduction

Multihadron production in soft hadron-hadron, hadron-nucleus and nucleus-nucleus collisions is one of the fields where serious predictions from quantum chromodynamics (QCD) are missing. These processes are dominated by unperturbative properties of QCD. Therefore different models are used to interpret the data. Especially high energy collisions of heavy ions offer the exciting possibility to discover experimentally a new state of matter, the quark gluon plasma [1–5]. However we should understand also the characteristics of such collisions within conventional low $p_\perp$ particle production. Models which have been successful extended from hadron-nucleus to nucleus-nucleus collisions are for example:

(*i*) the dual multi-chain parton fragmentation model [6, 7],

(*ii*) the additive quark model [8, 9],

(*iii*) the gluon exchange model [10, 11].

We study here the dual multi-chain fragmentation model, which starts from the dual topological unitarization scheme (DTU).

Capella and Tran Thanh Van developed a two-chain model for hadron-hadron interactions [12] on the basis of the DTU scheme and generalized it to a multi-chain model

* Presented at the XXIV Cracow School of Theoretical Physics, Zakopane, Poland, June 6–19, 1984.

for hadron-nucleus [13] and nucleus-nucleus collisions [6, 7]. This is the approach we already followed in Ref. [14], however, we formulated the model as a Monte-Carlo generator of exclusive events. The generation of Monte-Carlo events proceeds in two steps. In a first step a multi-chain event is generated. In the second step all chains fragment into stable hadrons according to a Monte-Carlo chain decay fragmentation model [15]. In this approach energy momentum and all additive quantum numbers are conserved exactly.

The talk is organized as follows: since a detailed description of the underlying model for hadron-hadron [14 a, b] hadron-nucleus [14 a, c] and nucleus-nucleus [14 d] collisions already exists, only a brief summary of the main features of these models is given in Section 2. In Section 3, 4 and 5 the Monte-Carlo results are compared to data from hadron--hadron, hadron-nucleus and nucleus-nucleus interactions or to results from alternative calculations, respectively. In Section 6 the conclusions are presented.

2. The underlying model

In hadron-scattering processes we assume that the interaction separates the valence quarks in each incident hadron into two colored systems. For an incident proton we obtain a quark and a diquark sharing the proton momentum. In the simplest version discussed here, we use only valence quarks. This gives rise to two multiparticle chains. In Figs. 1a, b and c all possible two-chain systems are shown for baryon-baryon, antibaryon-baryon and meson-baryon interactions. The energy or momentum fraction x carried by the single valence quarks contributing to a chain is obtained using valence quark distributions. In case of baryons the dressed diquark gets the remaining energy $1-x$, which corresponds to energy-momentum conservation on the parton level.

Building up the chains only from valence quarks is not correct for larger energies, i.e. at collider energies. In order to describe particle production at the energies of the CERN SPS collider we have to add further chains involving also sea quarks according to the AGK rules [16]. This has been done in Refs. [17, 18, 19].

In case of hadron-nucleus scattering the model becomes more complicated since many collisions occur. The average number of collisions ν inside the nucleus is given by the mass number A and the inelastic cross-sections for h-h and h-A interactions.

$$\bar{\nu} = A\sigma_{\text{inel}}^{\text{h-h}}/\sigma_{\text{inel}}^{\text{h-A}}. \tag{1}$$

In the calculations presented here we use inelastic cross-sections $\sigma_{\text{inel}}^{\text{h-h}}$ given in Ref. [20]. Each collision provides two chains like in hadron-hadron interactions. This gives rise to $2\bar{\nu}$ chains on the average. In order to construct 2ν chains we use not only valence quarks but also sea quarks from the projectile hadron. Taking into account only sea quarks from the projectile is of course not a good approach in case of very light target nuclei. In Fig. 2 an example of a triple-scattering process in a proton-nucleus collision is shown. The Fermi motion of the target nucleons is included according to the procedure described in Ref. [14 c].

Describing a nucleus-nucleus scattering process in such a model, one starts selecting the total number n of inelastic collisions taking place during the interaction and the num-

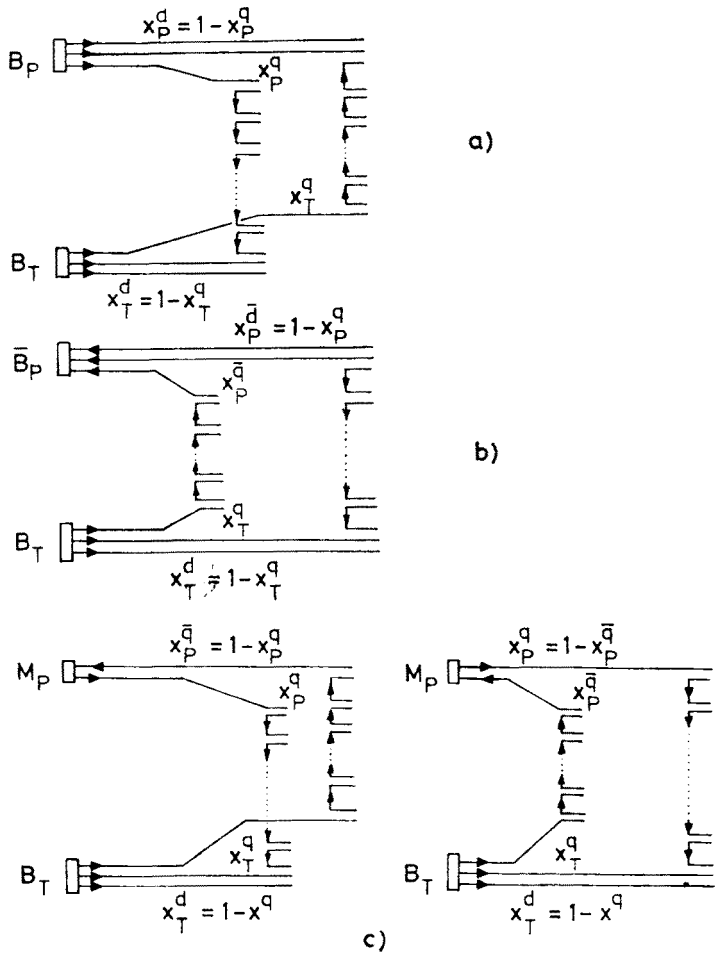

Fig. 1. All possible diagrams for two-chain systems in (a) baryon-baryon, (b) antibaryon-baryon and (c) meson-baryon interactions. B, $\bar{B}$, M stand for baryon, antibaryon and meson; x^q and x^d are the quark and diquark momentum fractions, respectively. The indices P and T stand for projectile and target particle

bers $n_A(n_B)$ of inelastically interacting nucleons of nucleus A(B). We sample n, n_A and n_B according to the cross section $\sigma_{AB}^{n_A,n_B,n}$ given in Ref. [6]. From the knowledge of n, n_A and n_B we can construct all our chains — altogether $2n$ chains. In difference to hadron-nucleus collisions we now have 3 types of chains: valence-valence chains, valence-sea chains and sea-sea chains. In Fig. 3 an example is given for the chain structure of a nucleus-nucleus scattering process with $n = 5$, $n_A = 2$ and $n_B = 3$.

The x-fractions of the valence quarks and sea quarks are sampled from valence and sea quark distributions in such a way, that energy-momentum conservation on the parton level is guaranteed also in case of hadron-nucleus and nucleus-nucleus interactions. Knowing the x-fractions of all quarks and diquarks we can easily calculate the invariant masses of each chain. The hadronization of the chains is handled for each chain separately on the

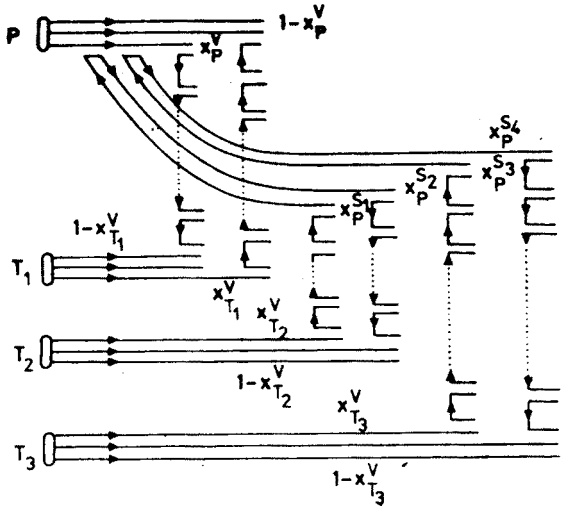

Fig. 2. Example of a triple-scattering diagram in a proton-nucleus interaction. P represents the incoming proton and T_1, T_2 and T_3 are the three target nucleons taking part at the interaction. x^V and x^S are valence and sea-quark momentum fractions

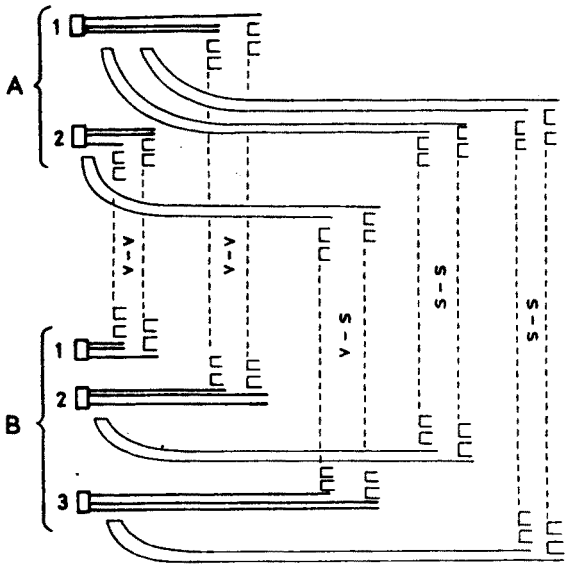

Fig. 3. Example for a nucleus-nucleus scattering process with $n = 5$ interactions and $n_A = 2$ contributing nucleons from nucleus A and $n_B = 3$ contributing nucleons from nucleus B. This gives rise to 4 valence--valence chains (v-v), 2 valence-sea chains (v-s) and 4 sea-sea chains (s-s)

basis of a Monte-Carlo chain decay fragmentation model [15] going into the centre of mass system of the considered chain.

After a Lorentz boost of all chains back into the laboratory frame of the hadron--hadron, hadron-nucleus or nucleus-nucleus collision we obtain a complete final hadronic

state conserving exactly energy-momentum and all additive quantum numbers. The conservation of these quantities is guaranteed, because our Monte-Carlo chain decay model conserves energy-momentum and additive quantum numbers during the hadronization process of each chain. Finally we consider the decay of hadron resonances into stable final hadrons using the Monte-Carlo code DECAY [21]. A more detailed description of the whole procedure as well as a discussion of the threshold behaviour of these three models is given in Ref. [14].

3. Comparison to data from soft hadron-hadron collisions

Since a detailed comparison to data on average multiplicities and multiplicity distributions has been already discussed in Ref. [14 a] we present here only x-distributions in the fragmentation region [22, 23], results on resonance production [24, 25] and forward--backward correlations [25].

In Fig. 4a, b we plot the inclusive cross section $x\frac{d\sigma}{dx}$ for the process $K^- + p \to \pi^\pm + X$ in the c.m. system for the target fragmentation region. The energy dependence as well as

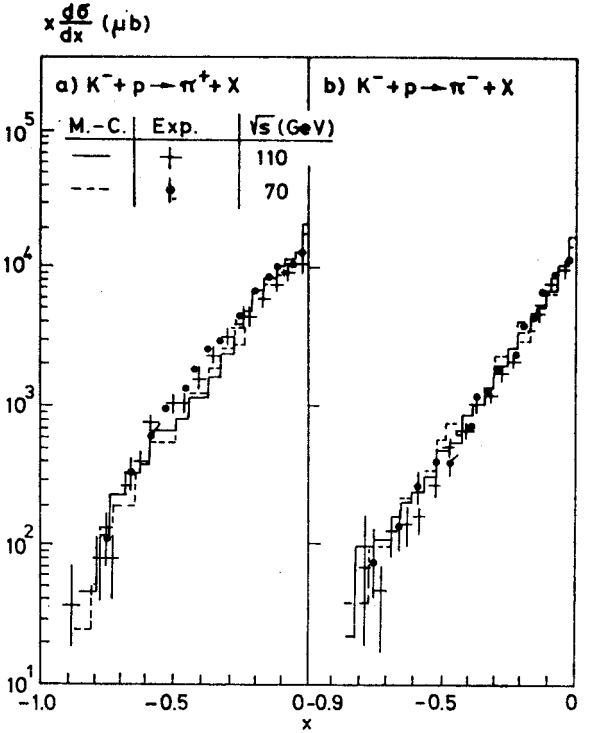

Fig. 4. Inclusive cross section $x\frac{d\sigma}{dx}$ (nb) plotted in the c.m. system for the processes (a) $K^- + p \to \pi^+ + X$ at $\sqrt{s} = 110$ GeV and $\sqrt{s} = 70$ GeV, (b) $K^- + p \to \pi^- + X$ at $\sqrt{s} = 110$ GeV and $\sqrt{s} = 70$ GeV. The Monte-Carlo results (histograms) are compared to data from Ref. [22]

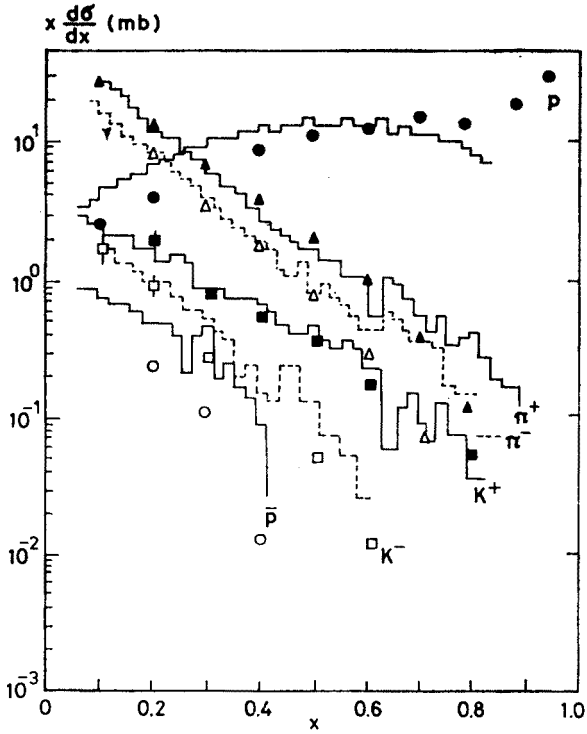

Fig. 5. Inclusive cross section $x\frac{d\sigma}{dx}$ (mb) for pp interactions into charged pions, charged kaons, protons and antiprotons at $p_{lab} = 175$ GeV/c plotted in the lab system. The Monte-Carlo results (histograms) are compared to data from Ref. [23]

the differences between π^+ and π^- distributions is well described by our two-chain Monte-Carlo model.

In Fig. 5 we show the inclusive longitudinal momentum distribution for pp-scattering into charged pions, kaons, protons and antiprotons in the lab frame at $p_{lab} = 175$ GeV/c. We get a good agreement to data [23] in the region $x \lesssim 0.6$. For larger x-values a comparison to data is problematic because we have not included diffractive particle production in the model. Furthermore we plot the $\sqrt{s}$ dependence for the multiplicity ratios $\langle\phi\rangle/\langle\varrho^0\rangle$ and $\langle\varrho^0\rangle/\langle\pi^-\rangle$ as well as the $p_\perp$-dependence of the ratio $\langle\varrho^0\rangle/\langle\pi^-\rangle$ at $\sqrt{s} = 63$ GeV measured in pp collisions, see Fig. 6, 7 and 8. In all three cases we get a reasonably well agreement to the data [24].

In Fig. 9 we show average ϱ^0-multiplicities versus the squared c.m. energy for π^+p and π^-p interactions and obtain also a good agreement to data presented in Ref. [25]. The inclusive x-distribution $x\frac{d\sigma}{dx}$ of ϱ^0 produced in K^-p reactions at $\sqrt{s} = 32$ GeV is given in Fig. 10. In the considered region $x \leqslant 0$ our two-chain model agrees well with the data [22].

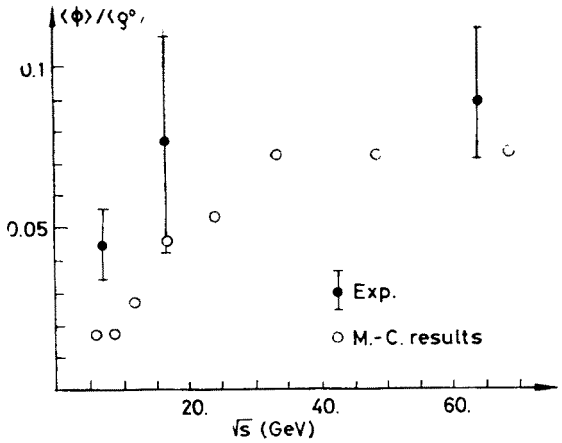

Fig. 6. $\sqrt{s}$ dependence of the average multiplicity ratio $\langle\phi\rangle/\langle\varrho^0\rangle$ for pp-interactions. The Monte-Carlo results, represented by crosses, are compared to data from Ref. [24]

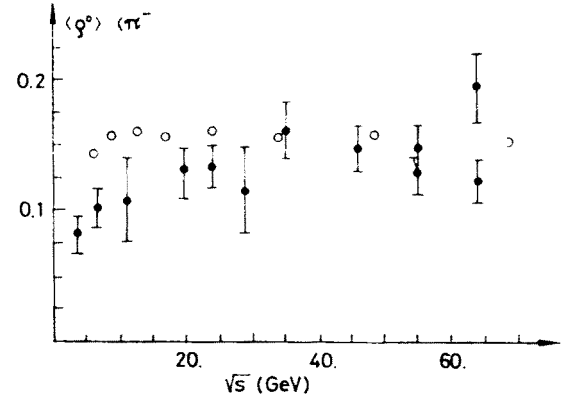

Fig. 7. The same quantity as in Fig. 6 but for the ratio $\langle\varrho^0\rangle/\langle\pi^-\rangle$

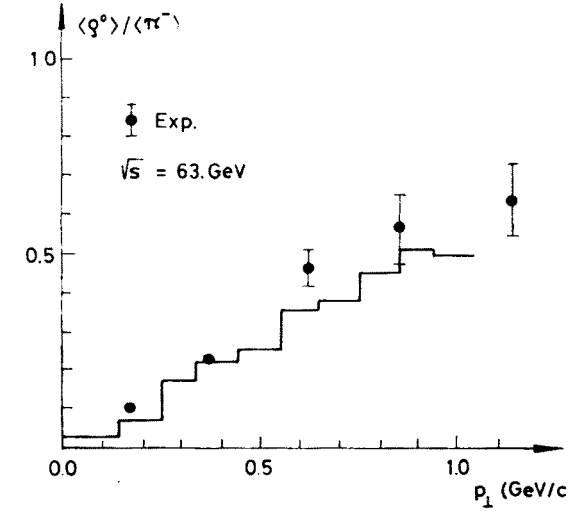

Fig. 8. $p_\perp$-dependence of the average multiplicity ratio $\langle\rho^0\rangle/\langle\pi^-\rangle$ for pp-interactions. The Monte-Carlo results (histograms) are compared to data from Ref. [24] measured at $\sqrt{s} = 63$ GeV

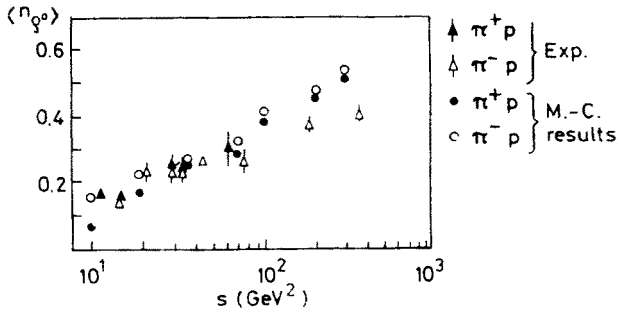

Fig. 9. Average multiplicities for (a) π^0, (b) ρ^0 versus the squared c.m. energy s measured in π^+p and π^-p reactions. The Monte-Carlo results are compared to data from Ref. [25]

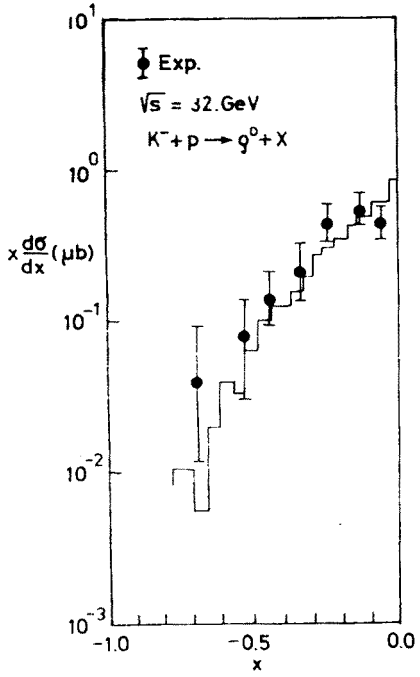

Fig. 10. The inclusive cross section $x\dfrac{d\sigma}{dx}$ for the process $K^-+p \to \rho^0+X$ at $\sqrt{s} = 32$ GeV plotted in the c.m. system. The Monte-Carlo results (histograms) are compared to data from Ref. [22]

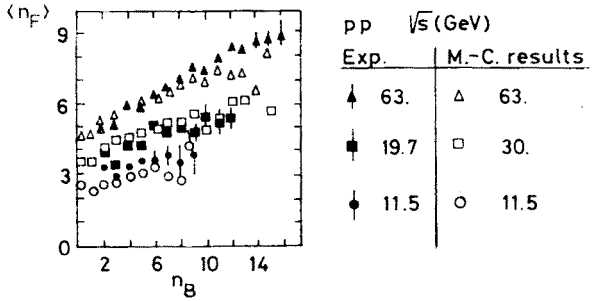

Fig. 11. $\langle n_F \rangle$ as function of n_B in pp-collisions at different c.m. energies. The Monte-Carlo results are compared to data presented in Ref. [25]

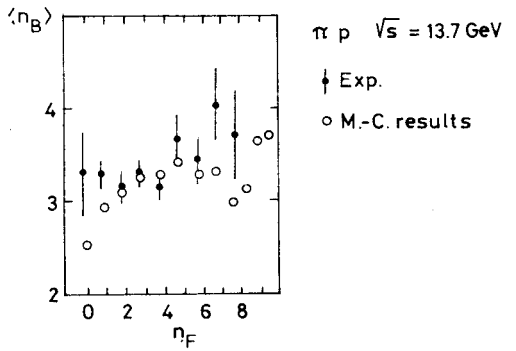

Fig. 12. $\langle n_B \rangle$ as function of n_F in π^-p-collisions at $\sqrt{s} = 13.7$ GeV. The Monte-Carlo results are compared to data presented in Ref. [25]

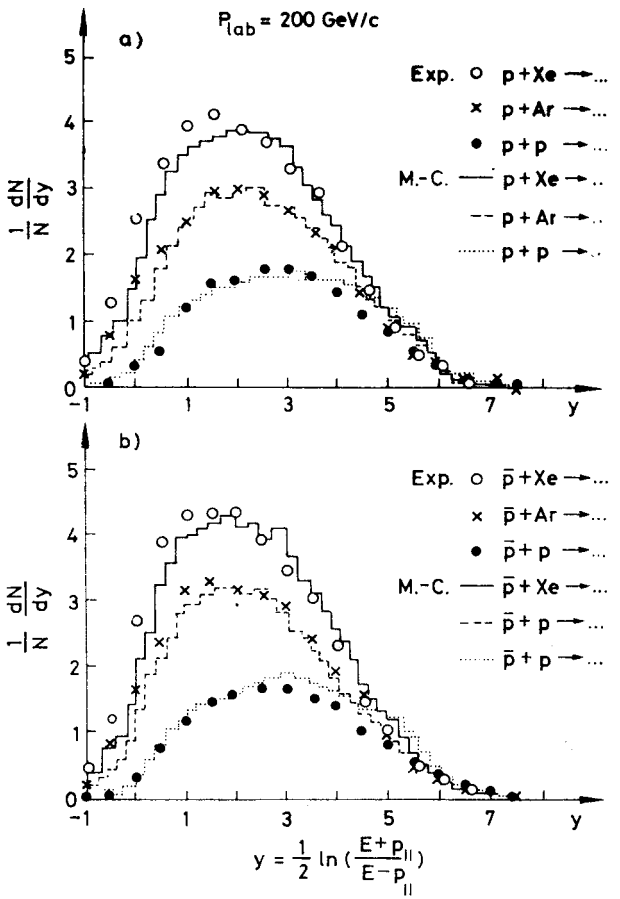

Fig. 13. Rapidity distributions dN/dy at $p_{lab} = 200$ GeV/c for (a) p Xe, p Ar and pp, (b) $\bar{p}$ Xe, p Ar and $\bar{p}$p interactions, the Monte-Carlo results (histograms) are compared to data from Ref. [27]

Finally in this Section, we consider in our two-chain model forward-backward correlations first studied in Ref. [26]. In Fig. 11 we show average forward multiplicity $\langle n_F \rangle$ versus the backward multiplicity n_B of proton-proton interactions at three different c.m. energies and in Fig. 12 we have plotted average backward multiplicities at $\sqrt{s} = 13.7$ GeV. Our Monte-Carlo results are compared to data measured in pp and π^-p collisions [25]. In both cases we obtain a reasonable agreement with the data.

4. Comparison to data from hadron-nucleus collisions

In Fig. 13 rapidity distributions are plotted at $p_{lab} = 200$ GeV/c for projectile protons and antiprotons and different targets. In case of nuclear targets the model provides a satisfactory description of the data [27] above $y \approx 1$. Below $y \approx 1$ the Monte-Carlo results are somewhat too low compared to the data. This might be due to additional nuclear effects, which are not included in our present model, such as the cumulative effect or the soft intra-

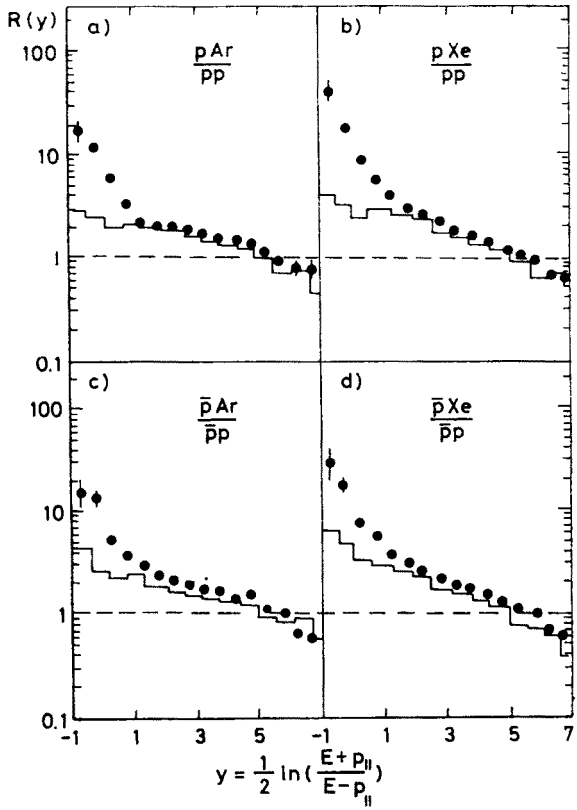

Fig. 14. Rapidity ratios $R(y) = dN/dy$ (hA)/dN/dy (hp) of all charged particles at $p_{lab} = 200$ GeV/c for (a) h = proton, A = Argon, (b) h = proton, A = Xenon, (c) h = antiproton, A = Argon, (d) h = antiproton, A = Xenon. The Monte-Carlo results represented by histograms are compared to data from Ref. [27]

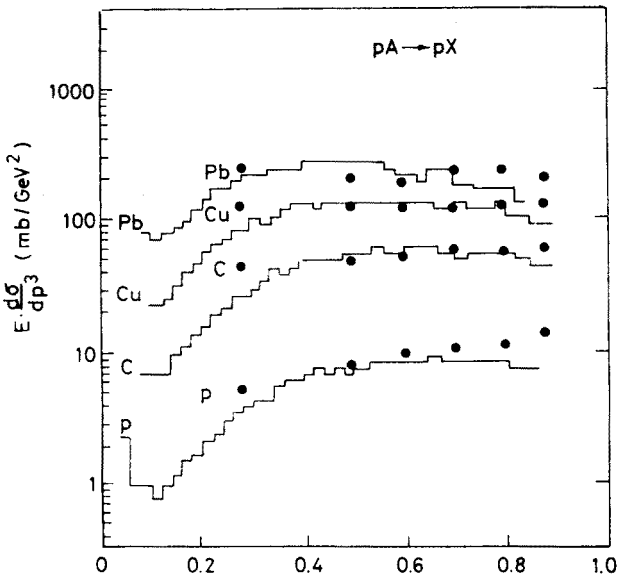

Fig. 15. The invariant differential cross section $E\,d\sigma/dp^3$ for pA → p+X as a function of x for an incident momentum of 100 GeV/c. The data [28] are measured at a fixed transverse momentum of $p_\perp = 0.3$ GeV/c. The Monte-Carlo results (40000 events) are represented by histograms

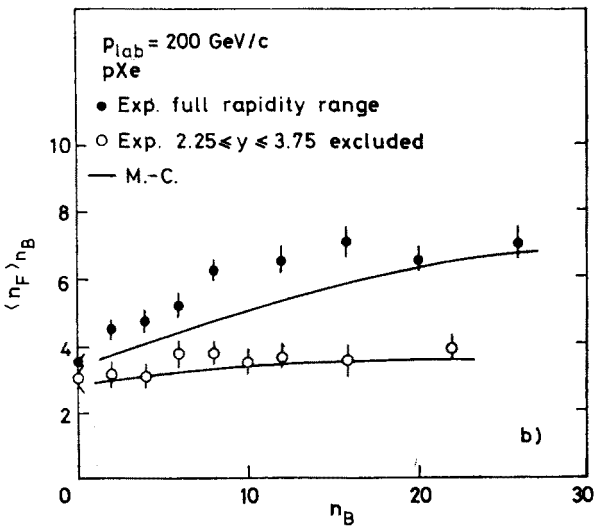

Fig. 16. The average multiplicity $\langle n_F \rangle$ in the forward hemisphere versus the multiplicity n_B in the backward hemisphere for p Xe reactions at $p_{lab} = 200$ GeV/c. All charged particles are considered. The Monte-Carlo results are compared to data from Ref. [27]

nuclear cascade. Rapidity distributions for pp and $\bar{p}p$ collisions are also shown in Fig. 13. In contrast to the experiment, our two-chain model for hadron-hadron interactions gives forward-backward symmetric distributions. This is what we expected. The difference between our model and the data [27] in the forward region could be caused by possible misidentifications of protons, antiprotons and kaons in the experiment. Since the particle misidentification for positively charged particles is approximately the same in pp and pA interactions, it is useful to consider the ratio of rapidity distribu ions

$$R(y) = \frac{dN}{dy}(\mathrm{hA}) \Big/ \frac{dN}{dy}(\mathrm{hh}).$$

The rapidity is defined as $y = \frac{1}{2} \ln [(E+p_{\|})/(E-p_{\|})]$. In Fig. 14a-d the ratio $R(y)$ for all charged particles is plotted for Argon and Xenon targets and incident protons and antiprotons. For $y \gtrsim 1$ the Monte-Carlo calculations agree reasonably well with the data [27]. In the region $y \lesssim 1$ our results are clearly below the data. In order to obtain a better agreement in the backward region as well, one would have to include further nuclear effects into the model.

In order to study the projectile fragmentation region in hadron-nucleus collisions, we plot in Fig. 15 the invariant cross section $Ed^3\sigma/d^3p$ for inclusive proton production as a function of the Feynman x-variable for Pb, Cu, C and H targets. Our model agrees reasonably well with the data [28] in the region $x \lesssim 0.8$. Since diffractive processes are not included in our Monte-Carlo model, we are not able to describe the data at larger x-values, $x \gtrsim 0.8$.

In Ref. [18, 19] it was found that forward-backward correlations are a sensitive test for the multistring nature of the model. These correlations in hadron-nucleus collisions were measured by De Mazro et al. [27]. In Fig. 16 we compare the forward multiplicity $\langle n_F \rangle$ versus the backward multiplicity n_B for p-Xe collisions. Strong correlations are seen. There is a good agreement of the model with the data. To exclude the effects of short range correlations the data are presented in Fig. 16 also after the elimination of the particles in the central region $2.25 \leqslant y \leqslant 3.75$. With this cut the correlations disappear. This expresses the fact that all additional sea-quark (projectile)/valence-quark (target) chains are at small rapidities in the lab frame and do not extend beyond $y = 3.75$. In this respect the model for hadron-nucleus collisions differs from the multi-chain hadron-hadron model [19], where the additional chains are centred around c.m.s. rapidity $y = 0$. Also this drastic decrease in the long-range correlations after the rapidity cut is well described by the model.

5. Comparison to cosmic ray data and to alternative calculations for nucleus-nucleus interactions

In Fig. 17 rapidity densities are plotted in the central region in dependence of the mass number B of the target nucleus. Our Monte-Carlo multi-chain model provides results for different projectile nuclei A, which are inbetween the results given in Ref. [6] and Ref. [9].

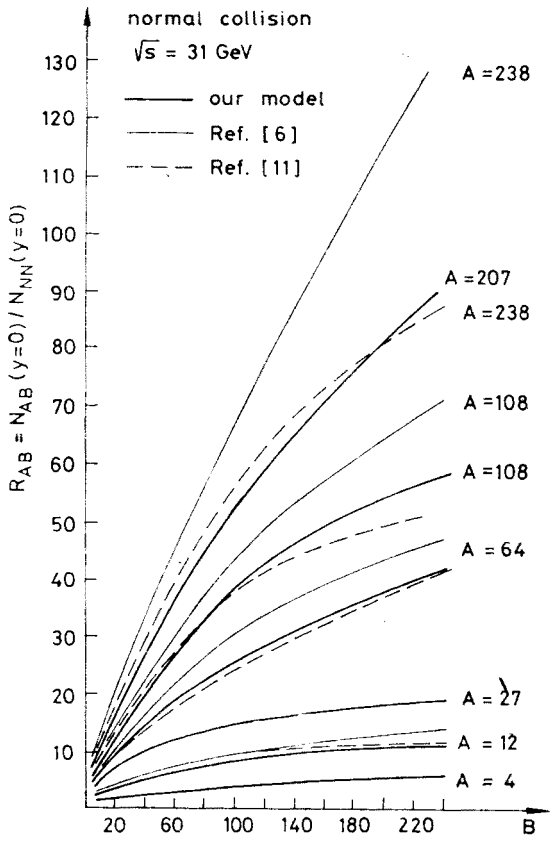

Fig. 17. Rapidity densities in the central region normalized to the nucleon-nucleon rapidity density. The Monte-Carlo results are compared to predictions from Refs. [6] and [9]

Fig. 18 contains the average negative particle multiplicity $\langle n_- \rangle = N_{AB}^{(-)}$ produced in A+B collisions at $\sqrt{s} = 31$ GeV as function of the target mass number B. $\sqrt{s}$ is the centre of mass energy of a nucleon-nucleon collision. Our model results also agree well with the predictions given in Ref. [6] and Ref. [11]. In Fig. 19 the same quantity is shown but for central collisions, following Ref. [6], we put $n_A = A$, which means, that all nucleons of the projectile nucleus A take part at the interaction. The principal reason for the difference of our results to the results of the same model as formulated by Capella et al. [6] is the form of our chain rapidity distributions which differs from that one given by Capella et al. [6]. This is due to the fact that we identify all particles in our calculations.

Furthermore we use kinematical corrections different from Ref. [6] in order to describe the threshold behaviour, see Ref. [14 d]. The differences between our model predictions and results from Ref, [6] give an impression of the dependence of such models on several parametrizations. Since these deviations are in the same order as deviations to results from other calculations [9, 11], we conclude that the differences presently obtained between such models are not significant. Pseudorapidity distributions are plotted in Fig. 20 a, b at

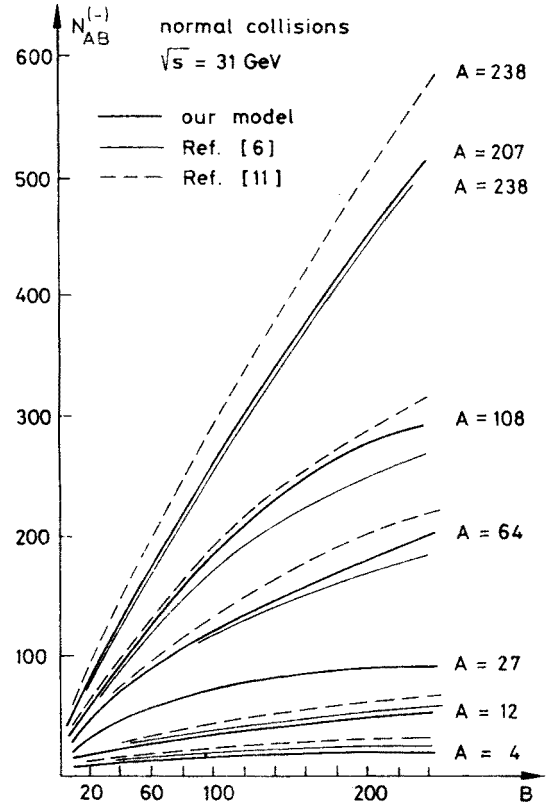

Fig. 18. Average negative particle multiplicity $\langle n_- \rangle = N_{AB}^{(-)}$. The Monte-Carlo results are compared to predictions from Refs. [6] and [11]

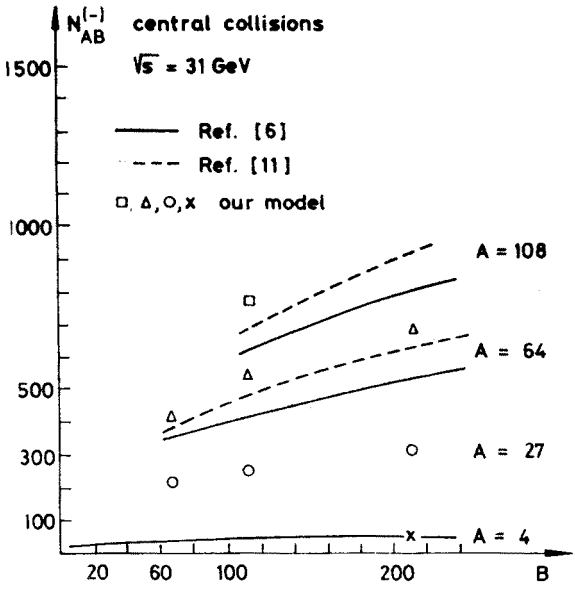

Fig. 19. Average negative particle multiplicity $\langle n_- \rangle = N_{AB}^{(-)}$ for central collisions. The Monte-Carlo results are compared to predictions from Refs. [6] and [11]

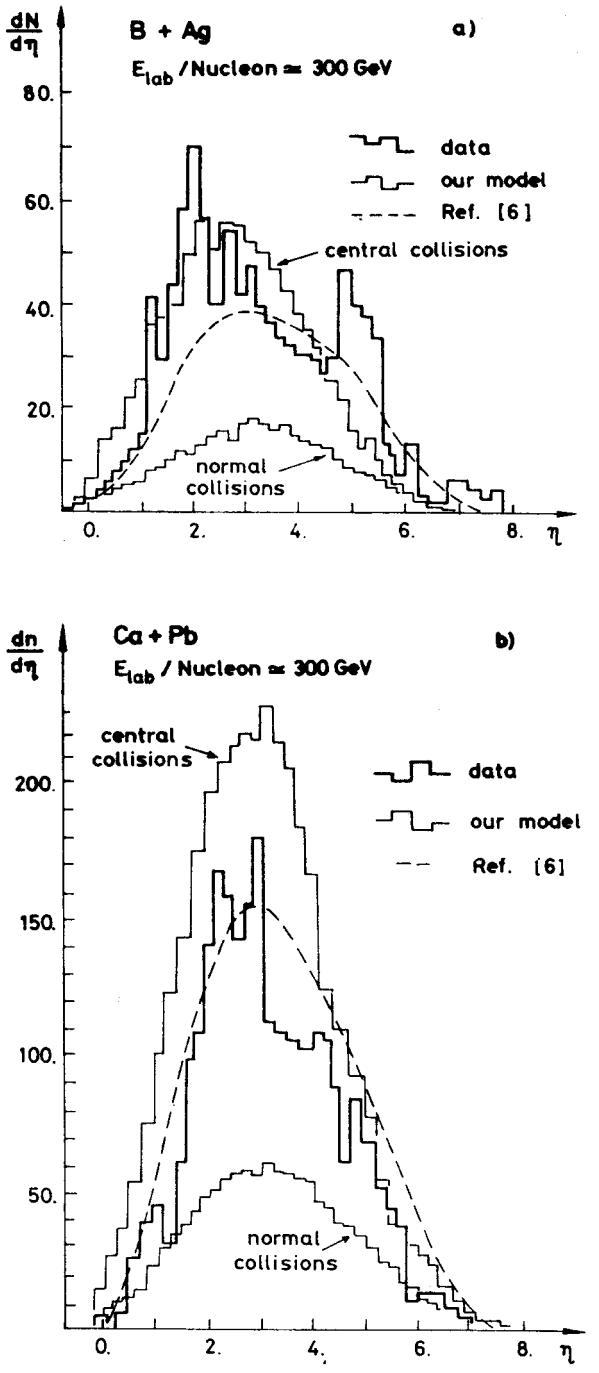

Fig. 20. Rapidity distributions for (a) B+Ag and (b) Ca+Pb collisions at $E_{\text{lab/nucleon}} \approx 300$ GeV. The Monte-Carlo results for normal and central collisions are compared to cosmic ray data [29] and predictions from Ref. [6]

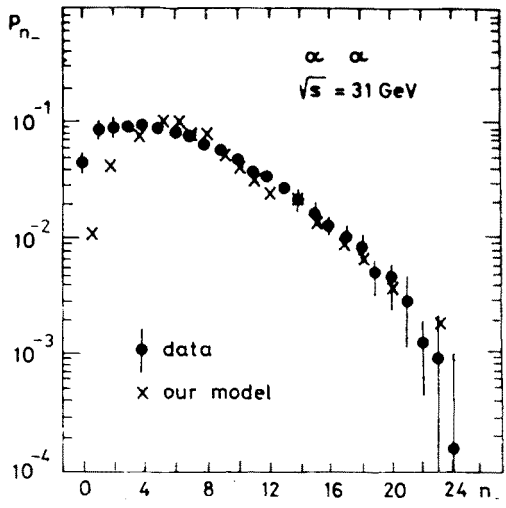

Fig. 21. KNO-distribution for negative particles in α–α collisions at $\sqrt{s} = 31$ GeV. The Monte-Carlo results are compared to data from Ref. [30]

$E_{\text{lab/nucleon}} = 300$ GeV for B+Ag and Ca+Pb collisions. Our model results for central collisions are compared to cosmic ray data [29] and model results from Ref. [6]. In general we have a reasonable agreement to the data.

Finally we plot in Fig. 21 the KNO-multiplicity distribution for negative multiplicities in $\alpha-\alpha$ collisions at $\sqrt{s} = 31$ GeV. Our model results for $n_- \gtrsim 4$ agree well with the data [30]. However, for $n_- \lesssim 4$ the Monte-Carlo points are below the data.

6. *Conclusions*

We have presented results of three models based on the dual parton model describing high energy hadron-hadron, hadron-nucleus and nucleus-nucleus collisions. Using a Monte-Carlo method allows us to calculate beside inclusive distributions also exclusive quantities. In this sense these models are well suited to generate complete exclusive events conserving energy-momentum and all additive quantum numbers.

In the case of our Monte-Carlo two-chain model for hadron-hadron collisions we continued our studies presented in Ref. [14a]. We get in general a good agreement to data on inclusive x-distributions, resonance production and forward-backward multiplicity correlations.

Average multiplicities, rapidity distributions and ratios as well as differential cross sections in the fragmentation region and forward-backward multiplicity correlations measured in hadron-nucleus collisions are also well described by our Monte-Carlo multi-chain model for hadron-nucleus interactions. Both models are not able to describe leading particle effects at x_F near 1 since we have not taken into account diffractive events.

Finally we presented first results of our nucleus-nucleus Monte-Carlo multi-chain

model for normal and central collisions. We obtained a reasonably good agreement to cosmic ray data and to results of other models. The differences between our calculations and these alternative calculations are not significant.

REFERENCES

[1] E. V. Shuryak, *Phys. Rep.* **61**, 71 (1980).

[2] M. Jacob, H. Satz eds., *Quark matter formation and heavy ion collisions*, Proc. of Bielefeld Workshop May 1982, World Scient. Publ. Co., Singapore 1982.

[3] L. Mc. Lerran, talk given at the XXII Int. Conf. on High Energy Physics, Leipzig, July 1984.

[4] R. Hagedorn, preprint CERN-TH 3684 (1983).

[5] M. Gyulassy, Berkeley preprint LBL 16800 (1983).

[6] A. Capella, C. Pajares, A. V. Ramallo, CERN preprint CERN-TH 3700 (1983).

[7] A. Capella, J. Kwiecinski, J. Tran Thanh Van, *Phys. Lett.* **108B**, 347 (1982); W. D. Chao, H. J. Pirner, *Z. Phys.* **C14**, 165 (1982).

[8] A. Białas, in Ref. [2]; V. V. Anisovich, Y. M. Shabelsky, V. M. Shekhter, *Nucl. Phys.* **135B**, 477 (1978); V. V. Anisovich, *Phys. Lett.* **57B**, 87 (1975); N. N. Nikolaev, *Phys. Lett.* **70B**, 95 (1977).

[9] A. Białas, A. Kolawa, *Acta Phys. Pol.* **B14**, 539 (1983).

[10] S. Brodsky, J. F. Gunion, J. H. Kuhn, *Phys. Rev. Lett.* **39**, 1120 (1977).

[11] S. Brodsky, Proc. of the 1st Workshop on ultrarelativistic nuclear collisions, LBL (1979).

[12] A. Capella, U. Sukhatme, C. I. Tan, J. Tran Thanh Van, *Phys. Lett.* **81B**, 68 (1979); A. Capella, U. Sukhatme, J. Tran Thanh Van, *Z. Phys.* **C3**, 329 (1980).

[13] A. Capella, J. Tran Thanh Van, *Phys. Lett.* **93B**, 146 (1980); *Z. Phys.* **C10**, 249 (1981).

[14] (a) J. Ranft, S. Ritter, *Z. Phys.* **C20**, 347 (1983); (b) J. Ranft, S. Ritter, submitted to *Z. Phys.* C; (c) J. Ranft, S. Ritter, CERN-TIS-RP 128 pp (1984), submitted to *Z. Phys.* C; (d) H.-J. Möhring, J. Ranft, S. Ritter, submitted to *Z. Phys.* C.

[15] J. Ranft, S. Ritter, *Acta Phys. Pol.* **B11**, 259 (1980); S. Ritter, *Z. Phys.* **C16**, 27 (1982); S. Ritter, *Comput. Phys. Commun.* **31**, 393 (1984).

[16] V. A. Abramovski, V. N. Gribov, D. V. Kancheli, *Yad. Fiz.* **18**, 595 (1971).

[17] A. B. Kaidalov, K. A. Ter-Martirosyan, *Phys. Lett.* **117B**, 247 (1982) and ITEP Moscow preprint 19651 (1983).

[18] A. Capella, J. Tran Thanh Van, *Phys. Lett.* **93B**, 146 (1980); *Phys. Lett.* **114B**, 450 (1982), *Z. Phys* **C18**, 85 (1983); *Z. Phys.* **C23**, 165 (1984), Orsay preprint LPTHE 83/10 (1983).

[19] P. Aurenche, F. W. Bopp, *Phys. Lett.* **114B**, 362 (1982); *Z. Phys.* **C13**, 459 (1982); P. Aurenche, F. W. Bopp, J. Ranft, *Z. Phys.* **C23**, 67 (1984) and CERN preprint CERN-TH 3775 (1983).

[20] H.-J. Möhring, CERN report TIS-RP/116 (1983).

[21] K. Hänßgen, S. Ritter, *Comput. Phys. Commun.* **31**, 411 (1984).

[22] R. Göttgens et al., CERN preprint CERN/EP 83-161 (1983).

[23] A. E. Brenner et al., Fermilab preprint, FERMILAB-PUB-81/82 Exp. (1982), submitted to *Phys. Rev.* D.

[24] C. W. Fabjan et al., *Nucl. Phys.* **B203**, 27 (1982).

[25] A. Wróblewski, Review talk at the XIV Int. Symp. on Multiparticle Dynamics, Granlibakhen, Lake Tahoe, USA, June 1983.

[26] A. Capella, J. Tran Thanh Van, *Z. Phys.* **C18**, 85 (1983).

[27] C. De Marzo et al., *Phys. Rev.* **D26**, 1019 (1982).

[28] A. E. Brenner et al., *Phys. Rev.* **D27**, 2580 (1983).

[29] Th. Barnett et al., *Phys. Rev. Lett.* **50**, 2062 (1983); S. Tasaka et al., 17th ICRC, Paris, July 1981, Vol. 5, p. 126.

[30] T. A. Kesson et al., *Phys. Lett.* **119B**, 245 (1982); W. Bell et al., CERN preprint CERN-EP/83-64 (1983).